Modelling Simul. Mater. Sci. Eng. **16** (2008) 035007 (19pp) doi:10.1088/0965-0393/16/3/035007

Modelling microstructure effects on the conduction in fibrous materials with fibre–fibre interface barriers

J-P Vassal, L Orgéas and D Favier

Laboratoire Sols-Solides-Structures-Risques (3SR), CNRS - University of Grenoble (INPG - UJF), BP 53, 38041 Grenoble cedex 9, France

E-mail: Laurent.Orgeas@hmg.inpg.fr

Received 17 November 2007, in final form 19 November 2007
Published 19 March 2008
Online at stacks.iop.org/MSMSE/16/035007

Abstract

Conduction in fibrous materials made of highly conductive fibres and immerged in a poorly conductive matrix is modelled above the percolation threshold. Firstly, limits of discrete approaches generally used to tackle this problem are determined on elementary fibrous microstructures by comparing discrete solutions with full finite element calculations. Then, more complex 3D fibrous microstructures are numerically generated and a discrete element code is used to analyse the influence of the fibre content, aspect ratio, orientation as well as the quality of fibre–fibre contacts on the effective conductivity tensor. Lastly, a semi-empirical analytical expression is proposed to model numerical results.

(Some figures in this article are in colour only in the electronic version)

1. Introduction

Due to their lightness and their rather low processing cost, thermally or electrically conductive polymer composites offer new possibilities for replacing metal parts in applications where heat and/or electric current have to be transported. Conductive composites can be obtained by incorporating into the poorly conductive polymer matrix highly conductive particles (metal, carbon particles etc). Danes *et al* [1] consider that thermally conductive polymer composites have to reach a thermal conductivity around 2 W m^{-1} K^{-1} in order to be regarded as interesting solutions. To reach this goal, composites must contain a very high content of conductive particles [1, 2]: particles have to form a connected network through which heat or current is mainly transported. In order to lower the particle content, the use of slender particles such as fibres seems to be an appropriate solution [1–8].

Even if heat or current propagation in heterogeneous materials has been studied for decades [9–13], predicting effective transport properties of composites reinforced with a high concentration of conductive fibres is still a challenging subject. Indeed, as fibres are highly conductive compared with the matrix, predictions given by the usual bounds [14, 15] may be

inaccurate [16]. Moreover, in this concentration regime, each fibre has at least one contact with another so that analytical models dedicated to (semi)dilute regimes [17–21] are inappropriate. At high particle content and high contrast between particles and matrix conductivities, a possible way to tackle the problem is to neglect conduction in the bulk matrix, except in the vicinity of particle–particle contacting zones [22–24]. Under such an assumption, many continuous or discrete numerical models have been established [4, 6, 23–27], allowing (i) to validate analytical models near the percolation threshold [6, 28–32], i.e. still at rather low fibre content and (ii) to analyse some microstructure effects on the effective conductivity. Among them, only fibre orientation, which can play an important role in composites' conductivity, has only been extensively considered by Cheng *et al* [26] with planar fibrous networks and very good fibre–fibre contacts.

Except for some empirical models [33, 34], very few analytical models are able to predict thermal conductivity in random or oriented highly conductive fibrous microstructures at high fibre contents. Taipalus *et al* [3] have successfully used the model proposed by Weber and Kamal [35] but this model is only suited for 2D microstructures and some fitting parameters are hard to get from the microstructure. Recently, starting from an upscaling process [36] and using discrete element simulations [37], new analytical models have been proposed for 3D fibrous microstructures [37]. Nevertheless, these analytical expressions are only suited for perfect fibre–fibre contacts or, on the contrary, for very resistive contacts. No model has been proposed for the intermediate situation.

Within that context, the purpose of this paper is (i) to further investigate from discrete element simulations links between microstructures and effective conductivity in 3D random or oriented fibrous materials made of straight fibres and (ii) to propose an analytical expression of the effective conductivity tensor for a large range of fibre contents, aspect ratios and orientations and for a large range of fibre–fibre contact qualities. For that purpose, the considered local physics and fibrous microstructure as well as the continuous and discrete models obtained in [36, 37] are briefly presented in sections 2 and 3, respectively. The validity of these discrete formulations is discussed by comparing results obtained on very simple microstructures with those given by full finite element calculation (section 4). Then, more realistic 3D fibrous microstructures are generated and a discrete element code is used to analyse the influence of the fibre content, aspect ratio, orientation as well as the quality of fibre–fibre contacts on the effective conductivity tensor (section 5). Finally, an analytical expression is proposed to model numerical results (section 6).

2. Physics at the fibre scale

We consider a fibrous medium of highly conductive fibres of isotropic conductivity λ plunged in a stagnant and poorly conductive matrix (conductivity $\lambda_m \ll \lambda$). The characteristic length of the fibrous medium considered is L. The volume fraction of fibres f is considered to be above the percolation threshold. For the sake of simplicity, fibres are slender cylinders of length l and cross section $S \ll l^2$, their volume being noted Ω. Each fibre f_α is oriented along a direction $\boldsymbol{e}_\alpha$. It is assumed that the structure can be described as a periodic assembly of N_R repetitions (see figure 1) of a representative elementary volume (REV) of the microstructure. The volume of the REV is noted Ω_R and its typical size l_R which is of the same order of magnitude as l, i.e. $l_R = \mathcal{O}(l)$. A good separation of scale is assumed, so that the scale separation parameter $\varepsilon = l/L$ is very small. The REV (see figure 2) is made up of a set $\mathcal{P}_R$ of identical fibres noted f_α. The fibre–fibre contact noted $i\alpha\beta$ represents the ith fibre–fibre contact in the REV, between fibre f_α and f_β. $\mathcal{C}_R$ represents the set of C_R fibre–fibre contacts in the REV, whereas $\mathcal{C}_\alpha$ is the set of contacts of the fibre f_α.

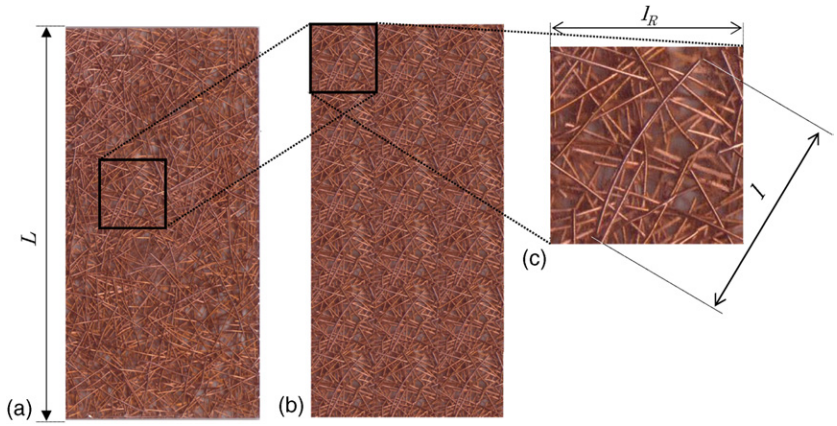

Figure 1. The following composite material is made up of conductive copper fibres plunged into a PMMA matrix (*a*). It can be represented by a periodic repetition (*b*) of N_R REVs (*c*).

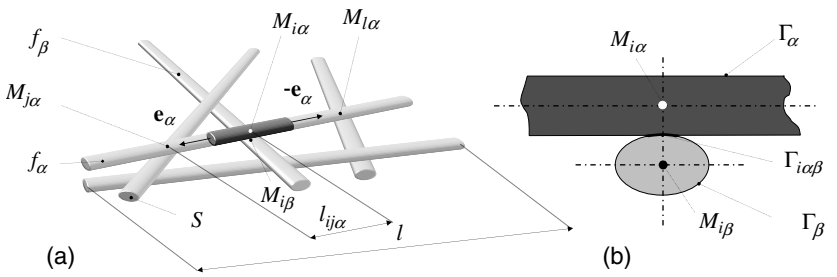

Figure 2. Scheme and notations used to define the considered fibrous microstructures: general view (*a*) and zoom on a contact zone (*b*).

The fibrous medium is subjected to a transient thermal loading, whose characteristic wave length is supposed to be of the same order of magnitude as L. Within each fibre f_α, the local thermal equilibrium reads:

$$C\frac{\partial T_\alpha}{\partial t} = -\boldsymbol{\nabla}\cdot\boldsymbol{q}_\alpha, \tag{1}$$

where T_α is the temperature field in the fibre, C its volumetric heat capacity and where the heat flow vector $\boldsymbol{q}_\alpha$ in the fibre follows Fourier's law:

$$\boldsymbol{q}_\alpha = -\lambda\boldsymbol{\nabla}T_\alpha. \tag{2}$$

As the conductivity of the matrix is supposed to be much smaller than the conductivity of fibres, conduction within the bulk matrix, i.e. far from fibre–fibre contact zones, are assumed to be negligible. Hence, far from fibre–fibre contact zones, the heat flow at the matrix–fibre interface Γ_α of local normal $\boldsymbol{n}_\alpha$ is supposed to be zero:

$$\boldsymbol{q}_\alpha\cdot\boldsymbol{n}_\alpha = 0. \tag{3}$$

Within fibre–fibre contact zones, in which typical cross sections are noted $\Gamma_{i\alpha\beta}$, heat transfers are considered to be due to conduction (i) through contact areas if fibres are in physical contact, (ii) through the matrix surrounding these physical contacts and (iii) through layers of entrapped matrix between almost touching fibres. To model such complex situations, a simple mixed

Cauchy type boundary condition is used in these zones:

$$\boldsymbol{q}_\alpha \cdot \boldsymbol{n}_\alpha = h_{i\alpha\beta}(T_\alpha - T_\beta), \tag{4}$$

where $h_{i\alpha\beta}$ are phenomenological heat transfer coefficients, assumed to be of the same order of magnitude, i.e. $h_{i\alpha\beta} = \mathcal{O}(h_c)$, where h_c is the characteristic heat transfer coefficient.

3. Physics at the macroscale

By using the homogenization method with multiple scale expansions [38–40], we have recently shown [37] that the macroscopic equivalent continuum corresponding to the above local physics is a one-phase medium, i.e. with a unique macroscopic temperature here noted T^e. It obeys a classical macroscopic heat balance equation:

$$C^e \frac{\partial T^e}{\partial t} = -\boldsymbol{\nabla} \cdot \boldsymbol{q}^e, \tag{5}$$

where the effective volumetric heat capacity $C^e = fC$ and the macroscopic heat flow $\boldsymbol{q}^e$ follows the standard Fourier's law:

$$\boldsymbol{q}^e = -\boldsymbol{\Lambda}^e \cdot \boldsymbol{\nabla} T^e, \tag{6}$$

where $\boldsymbol{\Lambda}^e$ is the effective conductivity tensor. Its computation requires the solving of steady-state and linear localization problems posed on REVs. The structure of these problems depends on the physics that controls conduction at the fibre scale. A relevant measure of the local physics is the following dimensionless Biot number:

$$\mathbb{B} = \frac{\Gamma_c h_c l_c}{S\lambda}, \tag{7}$$

where the characteristic scalars Γ_c, h_c and l_c can be respectively seen as averaged values of contact surfaces $\Gamma_{i\alpha\beta}$, heat transfer coefficients $h_{i\alpha\beta}$ and lengths of section of fibres contained between two adjacent fibre–fibre contacts. Hence, depending on the order of magnitude of $\mathbb{B}$, three models of effective conductivities have been obtained:

- For model III, which corresponds to $\mathbb{B} = \mathcal{O}(\varepsilon)$, fibre–fibre contacts are highly resistive, $\boldsymbol{\Lambda}^e$ does not depend on λ but is only a function of the heat transfer coefficients $h_{i\alpha\beta}$. Likewise, the localization problem exhibits a discrete form. It is a system of independent linear equations in which first order temperature fluctuations around T^e, i.e. $\varepsilon\bar{T}'_\alpha$, are unknown. These temperature fluctuations are constant in each fibre. For each fibre f_α (of centre of mass G_α) contained in the REV, one has to solve the following linear equation:

$$\sum_{\mathcal{C}_\alpha} \Gamma_{i\alpha\beta}\tilde{h}_{i\alpha\beta}((\varepsilon\bar{T}'_\beta - \varepsilon\bar{T}'_\alpha) + \boldsymbol{G}_\alpha\boldsymbol{G}_\beta \cdot \boldsymbol{\nabla} T^e) = 0, \tag{8}$$

  where $\tilde{h}_{i\alpha\beta}$ is the average of $h_{i\alpha\beta}$ over $\Gamma_{i\alpha\beta}$ and where the uniform macroscopic temperature gradient $\boldsymbol{\nabla} T^e$ is given and constant in the whole REV. Solving (8) then allows to compute the macroscopic heat flow with the following discrete expression:

$$\boldsymbol{q}^e = -\frac{1}{\Omega_R}\sum_{\mathcal{C}_R} \Gamma_{i\alpha\beta}\tilde{h}_{i\alpha\beta}((\varepsilon\bar{T}'_\beta - \varepsilon\bar{T}'_\alpha) + \boldsymbol{G}_\alpha\boldsymbol{G}_\beta \cdot \boldsymbol{\nabla} T^e)\,\boldsymbol{G}_\alpha\boldsymbol{G}_\beta. \tag{9}$$

- For model I, which corresponds to $\mathbb{B} = \mathcal{O}(1/\varepsilon)$, contacts are highly conductive. $\boldsymbol{\Lambda}^e$ only depends on λ. The localization problem to be solved for each fibre f_α reads:

$$\begin{cases} \left.\begin{array}{l} \boldsymbol{\nabla} \cdot \boldsymbol{q}'_\alpha = 0 \\ \boldsymbol{q}'_\alpha = -\lambda(\boldsymbol{\nabla}\varepsilon T'_\alpha + \boldsymbol{\nabla} T^e) \end{array}\right\} & \text{in } \Omega_f \\ \boldsymbol{q}'_\alpha \cdot \boldsymbol{n}_\alpha = 0 & \text{on } \Gamma_\alpha \\ \left.\begin{array}{l} \varepsilon T'_\alpha = \varepsilon T'_\beta \\ \boldsymbol{q}'_\alpha \cdot \boldsymbol{n}_{i\alpha\beta} = \boldsymbol{q}'_\beta \cdot \boldsymbol{n}_{i\alpha\beta} \end{array}\right\} & \text{on } \Gamma_{i\alpha\beta} \end{cases}, \tag{10}$$

where, once again, $\boldsymbol{\nabla} T^e$ is given and constant in the entire REV. The first order fluctuation temperatures $\varepsilon T'_\alpha$ are the unknowns to be determined. Solving (10) then allows us to compute the macroscopic heat flow:

$$\boldsymbol{q}^e = \langle \boldsymbol{q}'_\alpha \rangle = \frac{1}{\Omega_R} \sum_{\mathcal{P}_R} \int_\Omega \boldsymbol{q}'_\alpha \mathrm{d}V. \tag{11}$$

- For model II, $\mathbb{B} = \mathcal{O}(1)$, which corresponds to the intermediate physical situation, neither conduction in fibres nor heat transfer between fibres are dominating the physics at the microscale and the localization problem is identical to (10), except the condition on the contact zone, i.e. the fourth equation of the system (10) that now reads:

$$\boldsymbol{q}'_\alpha \cdot \boldsymbol{n}_{i\alpha\beta} = -h_{i\alpha\beta}(\varepsilon T'_\beta - \varepsilon T'_\alpha) \qquad \text{on } \Gamma_{i\alpha\beta}, \tag{12}$$

the expression of the effective heat flow (11) remaining unchanged.

Consequently, by imposing successively three independent unit macroscopic temperature gradients $\boldsymbol{\nabla} T^e$, the macroscopic conductivity tensor $\boldsymbol{\Lambda}^e$ can easily be obtained from (9) or (11). For instance, when $\boldsymbol{\nabla} T^e = \boldsymbol{e}_1$, one gets $\Lambda^e_{1i} = -q^e_i$ ($i \in \{1, 2, 3\}$).
One can finally notice that in the case of models I and II, systems of differential equations (10) have to be solved. In the following, these systems will be referred to as '*continuous formulations*'. Solving these localization problems can quickly become time consuming and cumbersome for realistic REVs. For that purpose, simplified discrete models have been proposed [37] when the aspect ratio of fibres is high enough to consider that heat flow is uniform in any cross section and mainly oriented along the fibres' centrelines. If these conditions are fulfilled, continuous localization problems (10) can be recasted to discrete systems of $2C_R$ (C_R for model I) linear equations. The $2C_R$ (C_R for model I) unknowns of the discrete problems are the first order temperature fluctuations $\varepsilon T'_{i\alpha}$ at nodes $M_{i\alpha}$, located on the centreline of fibre f_α, just in front of the contact $i\alpha\beta$ (see figure 2). For each node $M_{i\alpha}$, one has to solve the following discrete and linear heat balance equation:

$$\lambda S\left(\frac{\varepsilon T'_{j\alpha} - \varepsilon T'_{i\alpha}}{l_{ij\alpha}} + \boldsymbol{e}_\alpha \cdot \boldsymbol{\nabla} T^e\right) + \lambda S\left(\frac{\varepsilon T'_{l\alpha} - \varepsilon T'_{i\alpha}}{l_{il\alpha}} - \boldsymbol{e}_\alpha \cdot \boldsymbol{\nabla} T^e\right) + \Gamma_{i\alpha\beta}\tilde{h}_{i\alpha\beta}(\varepsilon T'_{i\beta} - \varepsilon T'_{i\alpha}) = 0, \tag{13}$$

where $l_{ij\alpha}$ is the length of the section (in the following, a section will define the part of a fibre included between two contacts) $ij\alpha$ of fibre f_α between nodes $M_{i\alpha}$ and $M_{j\alpha}$. The last term of the left-hand side of (13) is vanishing in the case of model I, in accordance with the fourth equation of system (10). This system will be next referred to as '*discrete formulation*'. By solving this problem, one can compute next the macroscopic heat flow (11) in a discrete form

$$\boldsymbol{q}^e = \frac{\lambda}{\Omega_R} \sum_{\mathcal{J}_R} \int_S \left(\frac{\varepsilon T'_{j\alpha} - \varepsilon T'_{i\alpha}}{l_{ij\alpha}} + \boldsymbol{e}_\alpha \cdot \boldsymbol{\nabla} T'^e\right) \boldsymbol{M}_{j\alpha} \boldsymbol{M}_{i\alpha} \, \mathrm{d}S + \frac{\tilde{h}_{i\alpha\beta}}{\Omega_R} \sum_{\mathcal{C}_R} \int_{\Gamma_{i\alpha\beta}} (\varepsilon T'_{i\alpha} - \varepsilon T'_{i\beta}) \boldsymbol{M}_{i\beta} \boldsymbol{M}_{i\alpha} \, \mathrm{d}S, \tag{14}$$

where $\mathcal{J}_R$ is the set of the $ij\alpha$ sections in the REV. As for the continuous formulation, the macroscopic conductivity tensor is easily deduced by solving successively the discrete

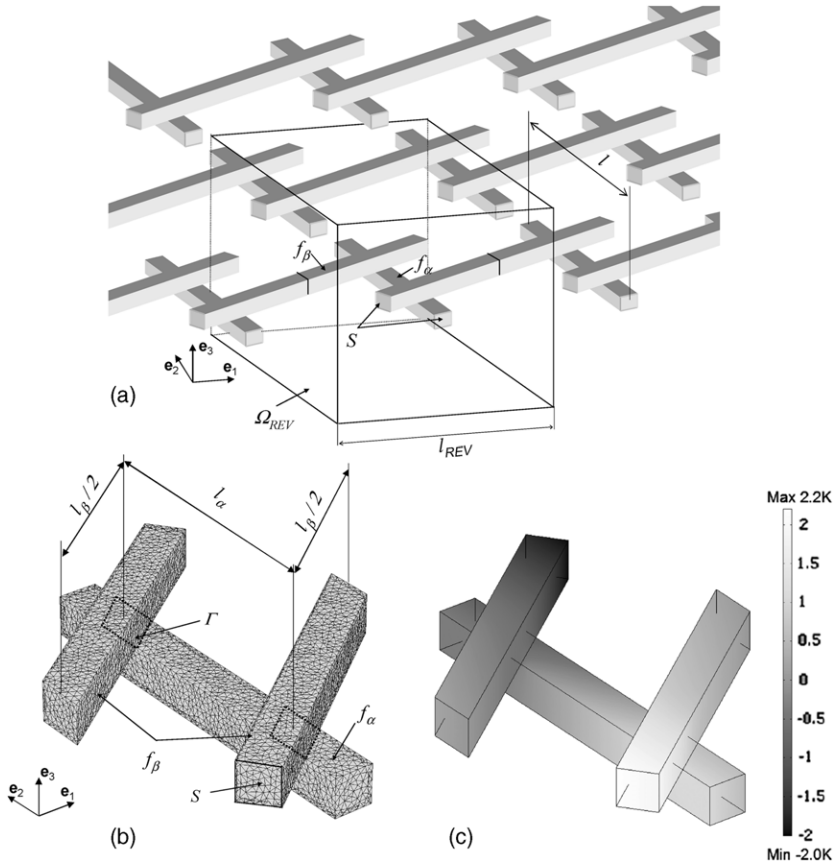

Figure 3. (*a*) Scheme of the elementary microstructures, only one vertical layer is represented. (*b*) Corresponding REV and associated FE mesh. (*c*) First order temperature fluctuation $\varepsilon T'$ (K) resulting from the FE calculation when the REV is subjected to a macroscopic temperature gradient $\nabla T^e = \boldsymbol{e}_1 (\mathrm{K\,m^{-1}})$.

system (13), for three independent unit macroscopic temperature gradients ∇T^e, and by calculating the macroscopic heat flow with (14).

4. Elementary fibrous microstructures

In this section, assumptions stated in order to establish the discrete formulations for models I and II are discussed with very simple fibrous microstructures. As seen in figure 3(*a*), the considered periodic REV is made up of only two fibres which form a percolating network in the $\boldsymbol{e}_1$ direction and whose centrelines belong to the plane $(\boldsymbol{e}_1, \boldsymbol{e}_2)$. Fibres are noted f_α and f_β. They have a length l and the centreline of the f_α fibre is aligned along $\boldsymbol{e}_2$. The length of the section between contact points $M_{1\alpha}$ and $M_{2\alpha}$ is noted $l_\alpha = 3l/6$, that between contact points $M_{1\beta}$ and $M_{2\beta}$ is noted $l_\beta = 5l/6$. Fibres exhibit a square cross section $S = d^2$. The two contact zones $\Gamma_{1\alpha\beta}$ and $\Gamma_{2\alpha\beta}$ are supposed to be well defined and have the same surface noted Γ. Moreover, a constant heat transfer coefficient h is used to model heat transfers through these two contact surfaces. Finally, the length l_R of the REV in the $\boldsymbol{e}_1$ direction is such that $l_\mathrm{R}^2 = l_\beta^2 - l_\alpha^2$. The other dimensions of the REV have been arbitrarily fixed to l_R. Hence, it is

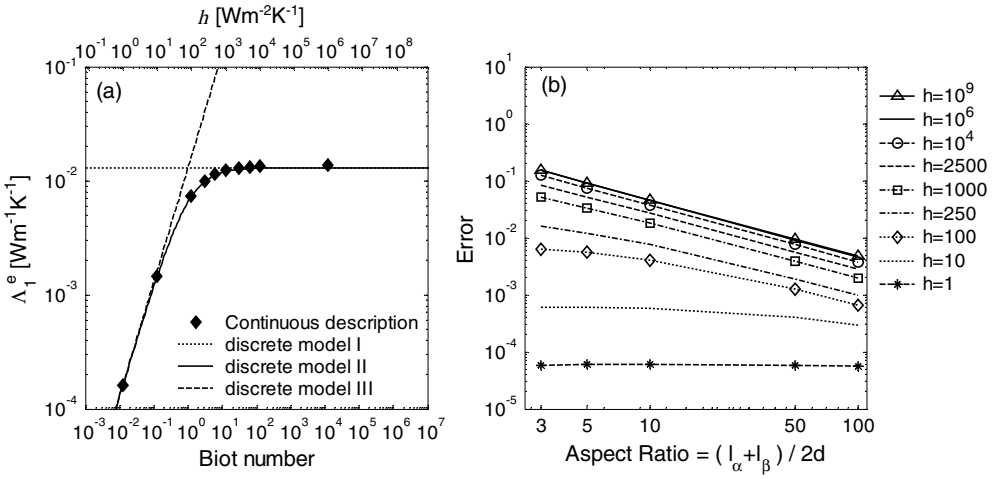

Figure 4. (*a*) Evolution of the effective thermal conductivity Λ_1^e with the Biot number $\mathbb{B}$ or the heat transfer coefficient h for an average aspect ratio of sections $(l_\alpha + l_\beta)/2d = 10$. Calculation made with continuous formulation for models I and II (black diamonds) and discrete formulation for all models (lines). (*b*) Influence of the average aspect ratio of active parts of fibres and heat transfer coefficient [W m^{-2} K^{-1}] on the error due to the discrete formulation.

possible to obtain easily from discrete formulations (13) (models I and II) and (8) (model III) analytical expressions of the effective conductivity tensor:

- Model I:

$$\boldsymbol{\Lambda}^e = \frac{1}{l_\mathrm{R}} \frac{S\lambda}{(l_\alpha + l_\beta)} \boldsymbol{e}_1 \otimes \boldsymbol{e}_1, \tag{15}$$

- Model II:

$$\boldsymbol{\Lambda}^e = \frac{1}{l_\mathrm{R}} \frac{S\Gamma\lambda h}{2S\lambda + h\Gamma(l_\alpha + l_\beta)} \boldsymbol{e}_1 \otimes \boldsymbol{e}_1, \tag{16}$$

- Model III:

$$\boldsymbol{\Lambda}^e = \frac{1}{2l_\mathrm{R}} \Gamma h \boldsymbol{e}_1 \otimes \boldsymbol{e}_1. \tag{17}$$

To check the validity of the above expressions, we have also solved the continuous formulation (10) on the same REVs using the commercial FE code Comsol [41] and computed the corresponding effective conductivity tensor. For that purpose, fibres were meshed with approximately 15 000 tetrahedra with quadratic polynomial interpolations, as shown in figure 3(*b*). Analytical and numerical results are compared in figure 4. The graph of figure 4(*a*) represents the evolution of the component Λ_{11}^e (equal to the principal component Λ_1^e, since the principal axes of the conductivity tensor $\boldsymbol{e}_\mathrm{I}$, $\boldsymbol{e}_\mathrm{II}$ and $\boldsymbol{e}_\mathrm{III}$ are aligned with $\boldsymbol{e}_1$, $\boldsymbol{e}_2$ and $\boldsymbol{e}_3$) of the macroscopic conductivity tensor with both h and $\mathbb{B} = \Gamma h(l_\alpha + l_\beta)/(2d^2\lambda)$, and both for the continuous and discrete formulations, when the mean aspect ratio of sections $(l_\alpha + l_\beta)/2d = 10$. Firstly, this graph shows that the discrete formulation of model II (continuous line) tends to the discrete formulation of model I (dotted line) when $\mathbb{B} \to \infty$ and to the discrete formulation of model III (dashed line) when $\mathbb{B} \to 0$. Secondly, one can notice that FEM simulation results obtained from continuous formulations of model I and II (black diamonds) follow the same trends as the discrete ones but are slightly higher. To further investigate this discrepancy, the graph plotted in figure 4(*b*) displays the evolution of the error

$(\Lambda_1^{e\ \text{Continuous}} - \Lambda_1^{e\ \text{Discrete}})/\Lambda_1^{e\ \text{Continuous}}$ when $(l_\alpha + l_\beta)/2d$ varies from 3 to 100. Results have been obtained for a wide set of heat transfer coefficients h, ranging from nearly perfect contacts ($h = 10^9\,\text{W m}^{-2}\,\text{K}^{-1}$) to very poor contacts ($h = 10^{-3}\,\text{W m}^{-2}\,\text{K}^{-1}$). As expected, the graph shows that the error quickly decreases when the aspect ratio increases. For example, in the case of perfect contacts, the error decreases from 15% to 0.5% when the aspect ratio of the section increases from 3 to 100. Moreover, the poorer the quality of contact is, the better the results of the discrete description are. It is important to note that the maximum error generated by the use of the discrete formulation remains rather weak, even for a small aspect ratio of the section (15% for an aspect ratio of 3). Consequently, within the investigated ranges of aspect ratios and heat transfer coefficients, physical assumptions used to establish discrete formulations for models I and II are relevant.

5. More complex fibrous microstructures

More complex and more realistic fibrous microstructures are now considered. Fibres are straight cylinders with identical length l and with a circular cross section of diameter d. Their aspect ratio is noted l/d. Fibrous REVs are generated numerically as previously [37,42]: fibres are supposed to be homogeneously distributed in cubic REVs of volume l_R^3 ($l_R \geqslant l$), the fibre orientation distribution function follows a Gaussian distribution, and a fibre–fibre contact is detected as soon as two fibres intersect. Typical fibrous networks generated with this procedure are illustrated in figure 5: even if a much more sophisticated generation procedure could have been used to obtain more realistic fibre–fibre contacts [31,32,43], the present microstructures are however quite close to those encountered in short fibres reinforced composites such as those shown in figure 1. Fibrous networks were built with various volume fraction of fibres f, fibre aspect ratios l/d and various fibre orientations, here characterized with the second order fibre orientation tensor $\boldsymbol{A}$ [44]. The microstructures have been generated so that the principal directions $\boldsymbol{e}_\text{I}$, $\boldsymbol{e}_\text{II}$ and $\boldsymbol{e}_\text{III}$ of the orientation tensor $\boldsymbol{A}$, are collinear with $\boldsymbol{e}_1$, $\boldsymbol{e}_2$ and $\boldsymbol{e}_3$ respectively. Hence, $A_{11} = A_\text{I}$, $A_{22} = A_\text{II}$ and $A_{33} = A_\text{III}$. For each set of microstructure parameters, ten REVs were generated. As illustrated in figure 5(d), the contact surface area $\Gamma_{i\alpha\beta}$ between two contacting fibres f_α and f_β is estimated as the intersection of the projected surfaces of the two contacting fibres on the plane perpendicular to the common normal to the two fibres' centrelines. For the sake of simplicity, the heat transfer coefficient h as well as the conductivity λ have been considered as constant for all fibre–fibre contacts and fibres, respectively. In order to explore links between the above microstructure parameters and effective thermal conductivity tensor, numerical experiments are performed using the discrete formulations that have been implemented in a discrete element code [37], initially developed to model the rheology of highly concentrated fibre suspensions [42,45].

5.1. Influence of the volume fraction of fibres

The influence of f has been studied in [37] in the case of models I and III and for constant area of fibre–fibre contacts equal to fibre cross section. In this situation, for high volume fractions, it has been observed that the effective conductivity was a linear function of the volume fraction of fibres when contacts are perfect (model I) while it was a quadratic function when contacts are of very poor quality (model III). In this work, (i) more realistic contacts, whose area accounts for the relative orientation of contacting fibres (see figure 5(d)), are considered and (ii) the situation where neither conduction in fibres nor the fibre–fibre contacts phenomenon dominates the conduction process (i.e. the situation corresponding to model II)

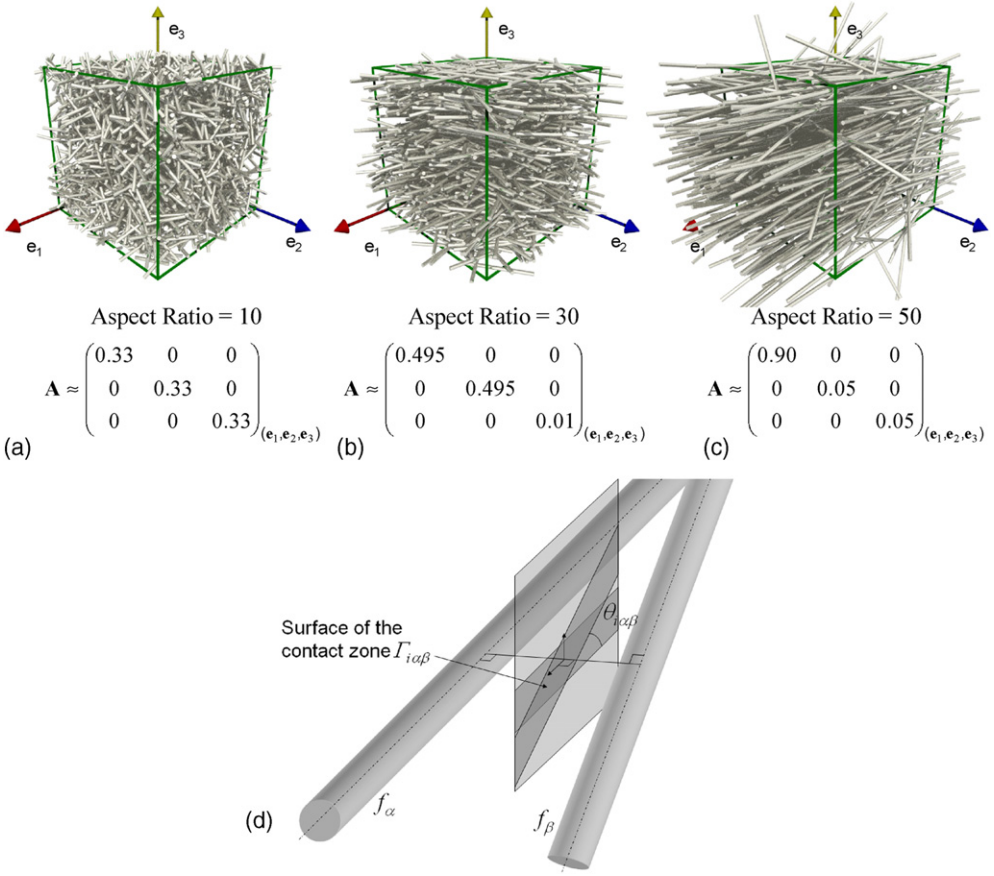

Figure 5. 3D random (*a*), planar random (*b*) and nearly unidirectional (*c*) generated fibrous REVs and their corresponding fibre aspect ratio and fibre orientation tensor. (*d*) Zoom on the surface contact between fibres f_α and f_β.

is studied. Results are presented in figure 6, in the case of isotropic networks of fibres exhibiting an aspect ratio $l/d = 50$. Only the first principal component Λ_1^e of the effective conductivity tensor is presented as similar results have been obtained for the other principal components. In figure 6(*a*), numerical results are represented by symbols. The volume fraction of fibres f varies from 0.01 to 0.4 and four heat transfer coefficients are considered: $h = 10^9\,\mathrm{W\,m^{-2}\,K^{-1}}$, $h = 100\,\mathrm{W\,m^{-2}\,K^{-1}}$, $h = 10\,\mathrm{W\,m^{-2}\,K^{-1}}$ and $h = 1\,\mathrm{W\,m^{-2}\,K^{-1}}$. The higher the heat transfer coefficient is, the higher the effective conductivity is. Moreover, below $f = 0.02$, no results can be obtained by the present method as the percolation threshold is close to this value (percolation threshold is estimated by Nan model [46] around $f = 0.014$). Lines plotted in figure 6(*a*) represent the best fits of the numerical data by power-laws: $\Lambda_1^e \approx af^n$. The values of coefficients a and n are given in the figure legend. For high volume fractions of fibres ($f \geqslant 0.05$) the quadratic evolution ($n = 2$) of the effective conductivity with the volume fraction obtained using model III in [37] is retrieved for heat transfer coefficient $h = 1\,\mathrm{W\,m^{-2}\,K^{-1}}$ (square symbols). When the heat transfer coefficient tends to infinity, the exponent n decreases and $n = 1.1$ for $h = 10^9\,\mathrm{W\,m^{-2}\,K^{-1}}$, so that the linear evolution of the effective conductivity tensor observed in [37] is almost retrieved. By contrast, results for $h = 10\,\mathrm{W\,m^{-2}\,K^{-1}}$ or $h = 100\,\mathrm{W\,m^{-2}\,K^{-1}}$ cannot be well

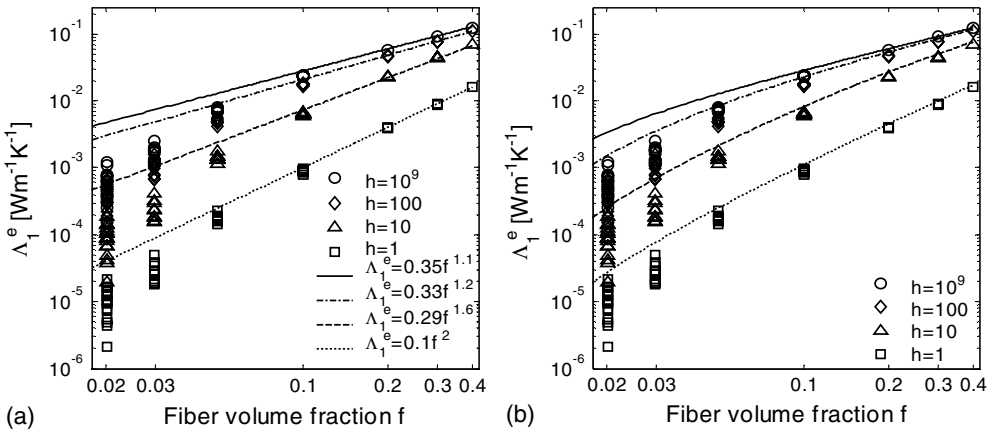

Figure 6. Influence of the volume fraction of fibres f on the first principal component of the effective conductivity tensor Λ_{I}^e (also noted Λ_{I}^e later, and equal Λ_{11}^e, since the principal axes of the conductivity tensor $\boldsymbol{e}_{\mathrm{I}}$, $\boldsymbol{e}_{\mathrm{II}}$ and $\boldsymbol{e}_{\mathrm{III}}$ are aligned with e_1, e_2 and e_3), for 3D random fibrous microstructures and for various values of the heat transfer coefficient h in ($\mathrm{Wm^{-2}\,K^{-1}}$). (*a*) Numerical results (symbols) have been fitted by power-laws (lines) and (*b*) compared with the hybrid model (equation (25)) (lines).

represented neither by a linear nor by a quadratic evolution, since $n = 1.6$ and $n = 1.2$, respectively.

5.2. *Influence of the fibre aspect ratio*

Figure 7 represents the variations of the three principal components Λ_i^e of the effective conductivity tensor when the aspect ratio of fibres l/d varies from 5 to 100. Results have been obtained for a fibre volume fraction of 0.2 and 3D random (figures 7(*a*, *b*, *c*)), planar random (figures 7(*d*, *e*, *f*)) or nearly unidirectional microstructures (figures 7(*g*, *h*, *i*)). The second order orientation tensor corresponding to these three types of microstructures are given in figure 5. Very conductive ($h = 10^9\,\mathrm{W\,m^{-2}\,K^{-1}}$ represented in figures 7(*a*, *d*, *g*)), very resistive ($h = 1\,\mathrm{W\,m^{-2}\,K^{-1}}$ represented in figures 7(*c*, *f*, *i*)) and intermediate ($h = 10\,\mathrm{W\,m^{-2}\,K^{-1}}$ represented in figures 7(*b*, *e*, *h*)) fibre–fibre contacts have been considered. In all cases, all components of $\boldsymbol{\Lambda}^e$ increase identically with the aspect ratio. The influence of the aspect ratio on $\boldsymbol{\Lambda}^e$ is much more pronounced when the contacts become less conductive. For example, in the case of 3D random microstructures, when l/d varies from 10 to 100, components of the effective conductivity tensor are multiplied approximatively by 3 when $h = 10^9\,\mathrm{W\,m^{-2}\,K^{-1}}$, by 30 when $h = 10\,\mathrm{W\,m^{-2}\,K^{-1}}$ and by 100 when $h = 1\,\mathrm{W\,m^{-2}\,K^{-1}}$.

5.3. *Influence of the fibre orientation*

In figure 7, one can also clearly gauge the strong anisotropy which is induced as microstructures display planar random or nearly unidirectional fibre orientation. In the case of perfect or extremely poor fibre–fibre contacts and for an aspect ratio l/d of 50, it has been shown [37] that the effective conductivity tensor $\boldsymbol{\Lambda}^e$ was almost a linear function of the second order fibre orientation tensor $\boldsymbol{A}$ whatever the fibre volume fraction is [37]. For intermediate situations ($h = 10\,\mathrm{Wm^{-2}\,K^{-1}}$) with $l/d = 50$, figure 8 represents the evolutions of the terms Λ_i^e/A_i ($i \in \{I, II, III\}$ no summation) with the fibre volume fraction for 3D random microstructures (figure 8(*a*)), planar random microstructures (figure 8(*b*)) and almost

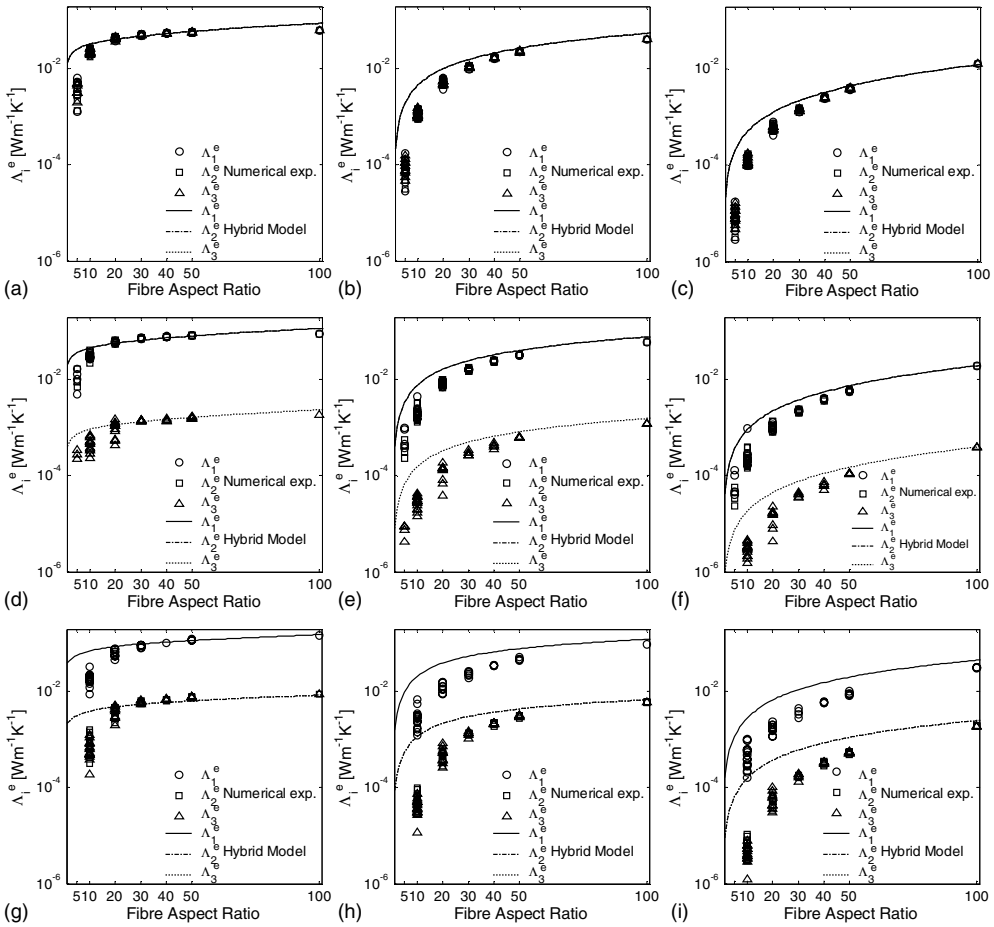

Figure 7. Influence of the fibre aspect ratio l/d on the principal components of the effective conductivity tensor Λ_i^e for 3D random (*a*)–(*c*), planar random (*d*)–(*f*) and nearly unidirectionnal (*g*)–(*i*) microstructures ($f = 0.15$), in cases of very conductive fibre–fibre contacts $h = 10^9\,\mathrm{W\,m^{-2}\,K^{-1}}$ (*a*), (*d*), (*g*), very resistive contacts $h = 1\,\mathrm{W\,m^{-2}\,K^{-1}}$ (*c*), (*f*), (*i*) and intermediate situation $h = 10\,\mathrm{W\,m^{-2}\,K^{-1}}$ (*b*), (*e*), (*h*). Numerical results (symbols) have been compared with the predictions given by the hybrid model (equation (25)) (lines).

unidirectional microstructures (figure 8(*c*)). The Λ_i^e/A_is are almost equal whatever the considered index i. A rather small discrepancy can be observed for almost unidirectionnal microstructures (figure 8(*c*)): when $f = 0.25$, the value of $\Lambda_{\mathrm{I}}^e/A_{\mathrm{I}}$ is approximately 10% lower than $\Lambda_{\mathrm{II}}^e/A_{\mathrm{II}}$ ($= \Lambda_{\mathrm{III}}^e/A_{\mathrm{III}}$). These results confirm that for intermediate quality of contacts, the effective conductivity tensor $\boldsymbol{\Lambda}^e$ can fairly be approximated as a linear function of the second order fibre orientation tensor $\boldsymbol{A}$.

Besides the influence of the in-plane anisotropy (defined as $A_{\mathrm{I}}/A_{\mathrm{II}}$, in the plane $(\boldsymbol{e}_1, \boldsymbol{e}_2)$) of the microstructure on its dimensionless through-plane conductivity (defined as $\Lambda_{\mathrm{III}}^e/\Lambda_{\mathrm{III}}^{e\,\mathrm{ISO}}$, where $\Lambda_{\mathrm{III}}^{e\,\mathrm{ISO}}$ is the through-plane conductivity for a 3D random microstructure) has been sketched in figure 9. Various through-plane microstructure anisotropies (defined as $(A_{\mathrm{I}} + A_{\mathrm{II}})/(2A_{\mathrm{III}})$) have been generated and very conductive ($h = 10^9\,\mathrm{W\,m^{-2}\,K^{-1}}$ see figure 9(*a*)), intermediate ($h = 10\,\mathrm{W\,m^{-2}\,K^{-1}}$ see figure 9(*b*)) as well as very poor contacts ($h = 1\,\mathrm{W\,m^{-2}\,K^{-1}}$ see figure 9(*c*)) have been studied. Results have been obtained here for

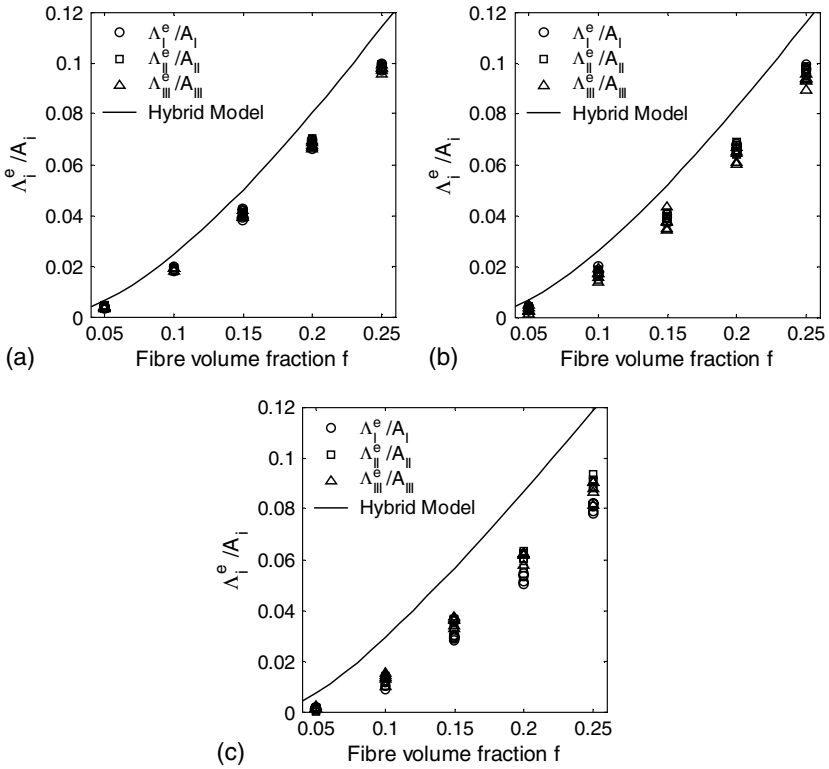

Figure 8. Evolutions of the scalar Λ_i^e/A_i's ($i \in \{I, II, III\}$ no summation) where $\mathbf{\Lambda}^e$ is the effective conductivity tensor and $\boldsymbol{A}$ is the second order orientation tensor. Evolutions are plotted as functions of the fibre content f for 3D random (*a*), 2D random (*b*) and almost unidirectional (*c*) microstructures with $h = 10\,\mathrm{Wm}^{-2}\,\mathrm{K}^{-1}$ and $l/d = 50$. Numerical results (symbols) have been compared with the predictions given by the hybrid model (equation 25) (lines).

a fibre volume fraction of 0.2 and an aspect ratio $l/d = 50$. This figure shows that the dimensionless through-plane conductivities are nearly constant when the in-plane anisotropy of the microstructure evolves. Only a slight decrease is recorded as the anisotropy increases: it is then fair to consider that, whatever the quality of fibre–fibre contacts is, the effective conductivity in a given direction is independent of the anisotropy of the microstructure in the directions normal to the considered one. This result is a consequence of the 'linearity' of the tensor $\mathbf{\Lambda}^e$ with the second order fibre orientation tensor $\boldsymbol{A}$ (see figure 8). This result is of great technical importance. Industrial processes of short fibre composites such as injection or compression moulding cause important variations of the orientation of fibres in the plane of the parts [47–49]. Nonetheless, microstructures are often almost planar so that their through-plane anisotropy can be considered as constant [48, 50]. Hence the last result presented in figure 9 tends to prove that the experimental variations of the through-plane conductivities in injected parts of short fibre composites observed by [5] cannot be a consequence of in-plane anisotropy of the microstructure.

5.4. Influence of the heat transfer coefficient

The influence of the heat transfer coefficient h on the effective conductivity is explored via the Biot number $\mathbb{B} = 4\tilde{\Gamma}h\tilde{l}/\lambda\pi d^2$, where $\tilde{\Gamma}$ and $\tilde{l}$ are the averaged values of contact surfaces and

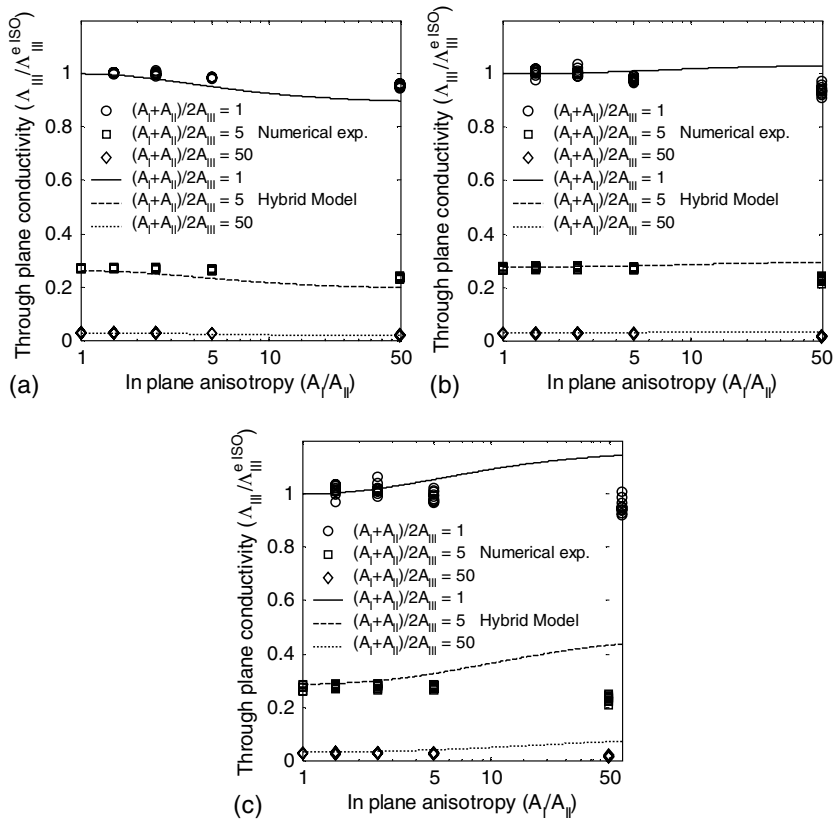

Figure 9. Evolution of the dimensionless through-plane conductivity with the in-plane anisotropy for the different through-plane anisotropies for $f = 0.2$ and $l/d = 50$ in cases of very conductive fibre–fibre contacts $h = 10^9\,\mathrm{W\,m^{-2}\,K^{-1}}$ (*a*), very resistive contacts $h = 1\,\mathrm{W\,m^{-2}\,K^{-1}}$ (*c*) and intermediate situation $h = 10\,\mathrm{W\,m^{-2}\,K^{-1}}$ (*b*). Numerical results (symbols) have been compared with the predictions given by the hybrid model (equation (25)) (lines).

lengths of section, respectively. Figure 10 presents the evolution of the principal components of the effective conductivity tensor with $\mathbb{B}$ for 3D random (figure 10(*a*)), planar random (figure 10(*b*)) and nearly unidirectional fibrous microstructures (figure 10(*c*)). These results are obtained here with a volume fraction of fibres $f = 0.2$ and with fibres presenting an aspect ratio $l/d = 50$. Three different zones can be considered:

- The first zone corresponds to small Biot numbers: $\mathbb{B} < 10^{-2}$. It is characterized by an effective conductivity increasing linearly with $\mathbb{B}$. In this situation the physics is dominated by conduction in the contact zones (model III).
- The second zone corresponds to intermediate Biot numbers: $10^{-2} < \mathbb{B} < 10^2$. In this zone, the effective conductivity is less sensitive to $\mathbb{B}$ (model II).
- The third zone corresponds to high Biot numbers: $\mathbb{B} > 10^2$. In this situation effective conductivity does not depend on the Biot number (model I).

It must be pointed out that these zones, which have already been identified for the elementary microstructure (cf figure 4(*a*)), do not depend on the fibre orientation distribution, fibre content and aspect ratio.

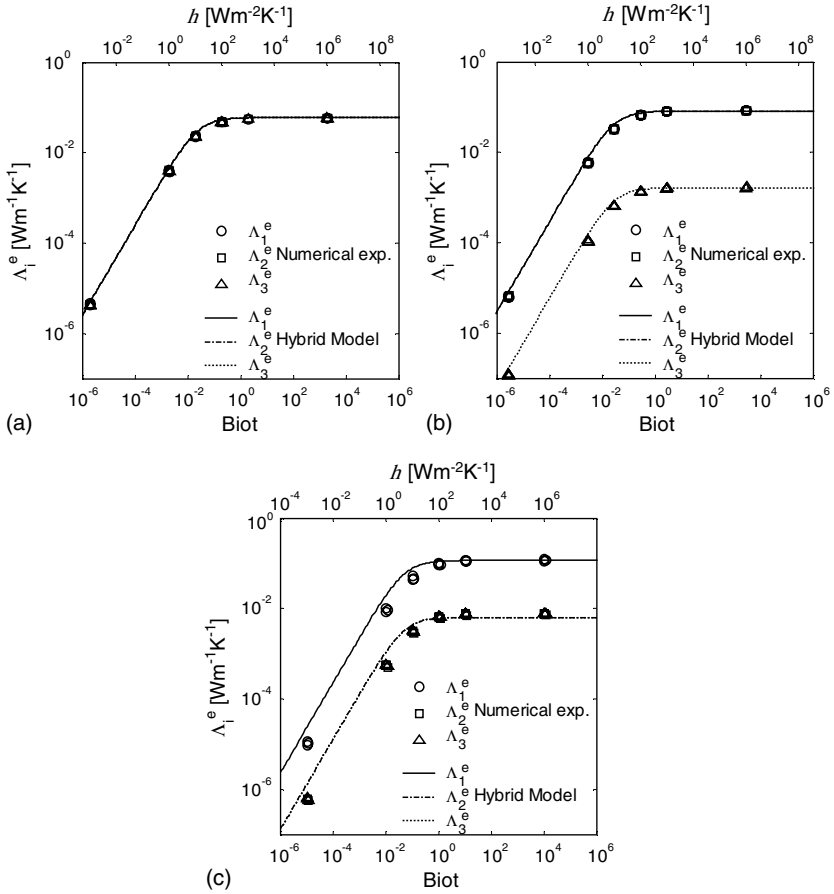

Figure 10. Evolution of the principal components Λ_i^e with the heat transfer coefficient h or the corresponding Biot number $\mathbb{B}$ for 3D random (*a*) planar random (*b*) and nearly unidirectional (*c*) microstrucutres ($f = 0.2$ and $l/d = 50$). Numerical results (symbols) are compared with the predictions given by the hybrid model (equation (25)) (lines).

5.5. Combined microstructure effects

As already underlined from the homogenization process [36], the Biot number $\mathbb{B}$ indicates the dominant local physics. It is a function of the heat transfer coefficient h (cf previous section) but it also depends on the mean length of fibre sections between contacts $\tilde{l}$ and the mean surface of contacts $\tilde{\Gamma}$. These microstructural parameters may depend on the fibre aspect ratio, content and orientation:

- Figure 11(*a*) presents the influence of the volume fraction of fibres f on the Biot number $\mathbb{B}$ for isotropic microstructures. The higher the volume fraction is, the higher the number of contacts per fibre is, so that the length of sections between contacts decreases and so the Biot number. Whatever the heat transfer coefficient is, the Biot number appears to be divided by 20 when the volume fraction of fibres increases from 0.02 to 0.4. Hence, when f increases, the effective conductivity may change from a physics corresponding to model II to a physics corresponding to model III (or from model I to model II).

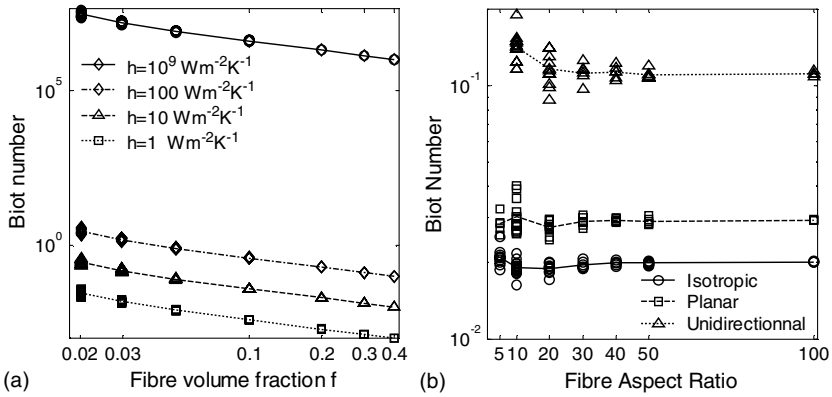

Figure 11. Evolution of the Biot number $\mathbb{B}$ with (a) the volume fraction of fibres f for various heat transfer coefficients (3D random REVs and $l/d = 50$) and with (b) the fibre aspect ratio l/d (for 3D random, planar random, and nearly unidirectional microstrucutres, $f = 0.2$) for very good fibre–fibre contacts.

- For a volume fraction of fibres $f = 0.2$, figure 11(b) represents the influence of the fibres' aspect ratio on the Biot number for isotropic, planar and unidirectional microstructures when the heat transfer coefficient $h = 10^9\,\mathrm{Wm^{-2}\,K^{-1}}$. The same trends have been observed for other heat transfer coefficients. Whatever the considered orientation or heat transfer coefficient, the aspect ratio seems to play no leading role on the Biot number.
- As shown in figure 11(b), a heat transfer coefficient of $10\,\mathrm{W\,m^{-2}\,K^{-1}}$ leads to Biot numbers around 0.02, 0.03 and 0.1, respectively for 3D random, planar random and unidirectional microstructures. Thus, for the same heat transfer coefficient (i.e. for the same quality of contacts), aspect ratio and fibre content, due to the variation of the surfaces of contacts with orientation, $\mathbb{B}$ is five times higher for oriented microstructures than for isotropic ones. The effective conductivity may change from a physics corresponding to model III to a physics corresponding to model II (or from model II to model I) when the microstructure becomes oriented.

6. Analytical hybrid model

From numerical results obtained in the previous section, a simple analytical model is proposed here to reproduce them. By considering that the temperature field within the fibrous medium follows an affine evolution, analytical expressions of the effective conductivity tensors have been proposed previously in the case of models I and III, for microsructures made up of homogeneously distributed straight and monodispersed fibres with circular cross section and identical area of contact [37]. Hence the effective conductivity tensor was estimated by

- in the case of model I:

$$\boldsymbol{\Lambda}^e \approx \boldsymbol{\Lambda}^{e\mathrm{I}} = f\lambda\left(1 - \frac{1}{\tilde{C}_\alpha}\right)\boldsymbol{A}, \tag{18}$$

- in the case of model III:

$$\boldsymbol{\Lambda}^e \approx \boldsymbol{\Lambda}^{e\mathrm{III}} = C_1 hk\pi\frac{d^2l^2}{24}\left(1 - \frac{1}{\tilde{C}_\alpha}\right)\boldsymbol{A}, \tag{19}$$

where $\tilde{C}_\alpha$ is the average number of contacts per fibre, C_1 is the number of contacts per unit of volume and $k = \tilde{\Gamma}/S$.

As shown in figure 5(*d*), the contact area $\Gamma_{i\alpha\beta}$ equals $d^2/\sin\theta_{i\alpha\beta}$, where $\theta_{i\alpha\beta}$ is the angle between the two contacting fibres f_α and f_β. Hence, by introducing $\langle\sin\theta\rangle$ as the average angle of the sine of angles $\theta_{i\alpha\beta}$ in the REV, one can obtain an estimate of k:

$$k = \frac{4}{\pi\langle\sin\theta\rangle}. \tag{20}$$

Finally, by assuming that fibres are homogeneously distributed in the REVs and that their orientation follows Gaussian distributions, it is possible to obtain, by using the statistical tube model [51–53], estimations of $\tilde{C}_\alpha$ and C_1:

$$\tilde{C}_\alpha \approx 4f\left(\frac{l}{\pi\frac{d}{2}}\phi_1 + \phi_2 + 1\right) \tag{21}$$

and

$$C_1 \approx \frac{f}{\pi dl}\tilde{C}_\alpha, \tag{22}$$

where the descriptors ϕ_1 and ϕ_2 can be calculated from the following discrete expression [37, 42]:

$$\phi_1 = \frac{1}{P_{\mathrm{R}}^2}\sum_{\mathcal{P}_{\mathrm{R}}}\sum_{\mathcal{P}_{\mathrm{R}}}\|\boldsymbol{e}_\alpha \times \boldsymbol{e}_\beta\|, \qquad \phi_2 = \frac{1}{P_{\mathrm{R}}^2}\sum_{\mathcal{P}_{\mathrm{R}}}\sum_{\mathcal{P}_{\mathrm{R}}}|\boldsymbol{e}_\alpha \cdot \boldsymbol{e}_\beta|. \tag{23}$$

The evolutions of ϕ_1, ϕ_2 and $\langle\sin\theta\rangle$ with the second order orientation tensor $\boldsymbol{A}$ have been numerically studied on microstructures with various fibre contents, aspect ratios and orientations. As an example, figure 12 shows the evolutions of these descriptors as functions of the two smallest principal values A_{I} and A_{II} of the fibre orientation tensor $\boldsymbol{A}$, for $f = 0.15$ and $l/d = 50$. Round symbols in figures 12(*a*)–(*c*) represent numerical results. Continuous surfaces plotted on the same graphs represent analytical estimations of the numerical results obtained from the following expressions:

$$\begin{aligned}
\phi_1 &= (-6.12A_{\mathrm{II}}^2 + 4.49A_{\mathrm{II}} - 2.49)A_{\mathrm{I}}^2 + (4.46A_{\mathrm{II}}^2 - 4.87A_{\mathrm{II}} + 2.23)A_{\mathrm{I}} - 2.47A_{\mathrm{II}}^2 \\
&\quad + 2.22A_{\mathrm{II}} + 0.14, \\
\phi_2 &= (-5.20A_{\mathrm{II}}^2 + 3.58A_{\mathrm{II}} - 1.07)A_{\mathrm{I}}^2 + (3.55A_{\mathrm{II}}^2 - 0.79A_{\mathrm{II}} - 1.26)A_{\mathrm{I}} + 1.09A_{\mathrm{II}}^2 \\
&\quad - 1.27A_{\mathrm{II}} + 1.00, \\
\langle\sin\theta\rangle &= (-6.85A_{\mathrm{II}}^2 + 5.23A_{\mathrm{II}} - 2.78)A_{\mathrm{I}}^2 + (5.10A_{\mathrm{II}}^2 - 5.50A_{\mathrm{II}} + 2.45)A_{\mathrm{I}} - 2.76A_{\mathrm{II}}^2 \\
&\quad + 2.44A_{\mathrm{II}} + 0.0839.
\end{aligned} \tag{24}$$

Such expressions allow fairly good fits of numerical results, whatever the investigated fibre content, aspect ratio and orientation ranges. Hence, purely analytical estimations of the macroscopic conductivity tensors in the case of models I and III can be obtained. In order to extend the validity domain of these two models to that of model II, the following phenomenological *hybrid model* is proposed:

$$\boldsymbol{\Lambda}^e \approx \boldsymbol{\Lambda}^{e\mathrm{II}} \approx \frac{1}{2}\left(\frac{1}{1 + 10\tilde{C}_\alpha f\mathbb{B}}\boldsymbol{\Lambda}^{e\mathrm{III}} + \frac{1}{1 + \dfrac{1}{10\tilde{C}_\alpha f\mathbb{B}}}\boldsymbol{\Lambda}^{e\mathrm{I}}\right), \tag{25}$$

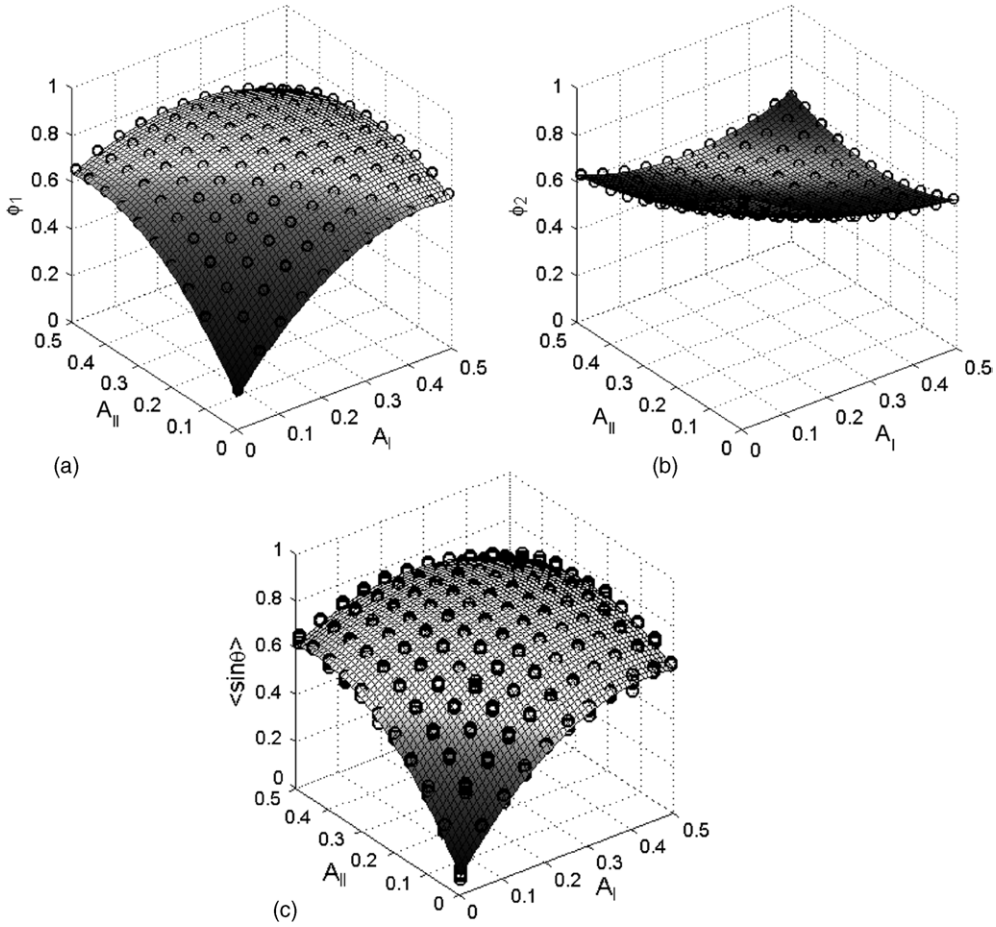

Figure 12. Evolution of the microstructure descriptors ϕ_1 (*a*), ϕ_2 (*b*) and $\langle \sin\theta \rangle$ (*c*) with the two minor principal values A_{I} and A_{II} of the second order fibre orientation tensor $\boldsymbol{A}$. The round symbols have been obtained from numerical generation (here $f = 0.15$). The continuous surfaces correspond to analytical expressions (24).

where $\boldsymbol{\Lambda}^{e\mathrm{I}}$ and $\boldsymbol{\Lambda}^{e\mathrm{III}}$ are calculated using equations (18) and (19), respectively. The Biot number involved in the above proposition can be estimated by:

$$\mathbb{B} \approx \frac{khl}{\tilde{C}_\alpha \lambda}, \tag{26}$$

where k is obtained from (20). Please note that when $\mathbb{B} \to \infty$ the above hybrid model numerically tends to model I, whereas it tends to model III when $\mathbb{B} \to 0$.

Predictions of the hybrid model (25) have been reported (lines) in figures 6(*b*), 7–10. The analysis of these figures brings up the following comments:

- Predictions follow qualitatively trends given by numerical results: the influence of various microstructure parameters is well captured.
- When fibre–fibre contacts are highly conductive, i.e. when $\mathbb{B} \to \infty$, and whatever the considered fibre orientation, predictions given by the hybrid model are quantitatively in good agreement with numerical results, if the fibre content f and aspect ratio l/d are higher than 0.05 and 20, respectively. Two possible factors can explain the observed

discrepancies below these values. Firstly, at lower fibre content, the generated REVs may not follow exactly the statistical tube model so that the number of contacts per unit of volume $\tilde{C}_\alpha$ involved in (18) may be lower than that predicted by the tube model. Secondly, the affine assumption used to build the analytical model I, may be more questionable for those low fibre contents.

- For intermediate situations, i.e. for intermediate Biot number, predictions are still satisfactory in the case of 3D random and planar random fibrous REVs, if $f \geqslant 0.05$ and $l/d \geqslant 20$. However, for nearly undirectional REVs, some deviation from the numerical results occurs. This discrepancy becomes more and more pronounced as $\mathbb{B} \to 0$. Reasons given in the previous points may explain it. Another possible explanation can also be formulated in this case. Indeed, it has been previously shown that the unique use of $\boldsymbol{A}$ in the analytical model III was not sufficient to obtain accurate predictions of numerical results for very oriented fibrous networks: better analytical estimations would be gained by accounting for the relative position and orientation of contacting fibres [37].

7. Concluding remarks

In this study, the transient diffusion equation through fibrous media with highly conductive fibres and interface barriers at fibre–fibre contacts has been considered. By studying the effective conductivity on elementary fibrous microstructures, and by comparing results given by simple discrete models and those obtained from full finite element calculations, we have first shown that the error induced by discrete estimations was rather small even for fibres' sections between contacts that do not display a large aspect ratio. Moreover, the lower the quality of fibre–fibre contacts, the lower this error is.

Therefrom, the effective conductivity of fibrous networks rather close to those encountered in short fibre polymer composites was investigated. More precisely, the influences of the fibre content, aspect ratio and orientation, as well as the quality of fibre–fibre contacts were studied:

- Depending on the quality of fibre–fibre contacts, the influence of the fibre content is drastic, following power-laws for contents above 0.05, the power law exponent ranging from 1 for perfect fibre–fibre contacts to 2 for highly resistive ones.
- In general, the effective conductivity tensor displays anisotropy, which can be considered as a linear function of the anisotropy of the second order fibre orientation tensor. The last result must be reconsidered as fibrous REVs becomes very oriented and fibre–fibre contacts become very resistive [37].
- For various fibre orientations and contents, and various qualities of contacts, the higher the fibre aspect ratio is, the higher the effective conductivity is. Moreover, the effective conductivity is more sensitive to the fibre aspect ratio in the case of resistive contacts.

Finally, an analytical hybrid model was proposed for the effective conductivity tensors. This model is devoted to REVs in which fibres are homogeneously distributed and follow Gaussian fibre orientation distributions. Despite its simplicity, its ability to reproduce discrete numerical simulations was checked within a large range of heat transfer coefficients, fibre contents, aspect ratios and orientations.

Acknowledgments

JPV would like to thank the Région Rhône-Alpes (France) for its support of this work through the research grant it provided.

References

[1] Danes F, Garnier B and Dupuis T 2003 *Int. J. Thermophys.* **24** 771
[2] Keith J, Hingst C, Miller M, King J and Hauser R 2006 *Polym. Compos.* **27** 388
[3] Taipalus R, Harmia T, Zhang M and Friedrich K 2001 *Compos. Sci. Technol.* **61** 801
[4] Wang C-W, Cook K A and Sastry A M 2003 *J. Electrochem. Soc.* **150** 385
[5] Danes F, Garnier B, Dupuis T, Lerendu P and Nguyen T-P 2005 *Compos. Sci. Technol.* **65** 945
[6] Dalmas F, Dendievel R, Chazeau L, Cavaillé J-Y and Gauthier C 2006 *Acta Mater.* **54** 2923
[7] Kim Y, Hayashi T, Endo M, Gotoh Y, Wada N and Seiyama J 2006 *Scr. Mater.* **54** 31
[8] Agari Y, Ueda A and Nagai S 1991 *J. Appl. Polym. Sci.* **43** 1117
[9] Kaviany M 1991 *Principles of Heat Transfer in Porous Media* (New York: Springer)
[10] Torquato S 2001 *Random Heterogeneous Materials* (New York: Springer)
[11] Milton G 2002 *The Theory of Composites* (Cambridge: Cambridge University Press)
[12] Sahimi M 2003 *Heterogeneous Materials* vol 1 and 2 (New York: Springer)
[13] Mawxell J-C 1954 *A Treatise on Electricity and Magnetism* 3rd edn (New York: Dover) p 1891
[14] Hashin Z and Shtrikman S 1962 *J. Appl. Phys.* **33** 3125
[15] Willis J 1977 *J. Mech. Phys. Solids* **25** 185
[16] Kim I and Torquato S 1993 *J. Appl. Phys.* **74** 1844
[17] Rocha A and Acrivos A 1973 *Q. J. Mech. Appl. Math.* **26** 441
[18] Batchelor G K 1974 *Annu. Rev. Fluid Mech.* **6** 227
[19] Shaqfeh E S G and Koch D L 1988 *Phys. Fluids* **31** 728
[20] Mackaplow M B, Shaqfeh E S G and Schiek R L 1994 *Proc. R. Soc. Lond.* A **447** 77
[21] Sundararajakumar R R and Koch D L 1997 *J. Non-Newtonian Fluid Mech.* **73** 205
[22] Batchelor G, O'Brien F and O'Brien R 1977 *Proc. R. Soc. Lond.* A **355** 313
[23] Cheng G, Yu A and Zulli P 1999 *Chem. Eng. Sci.* **54** 4199
[24] Cheng X and Sastry A 1999 *Mech. Mater.* **31** 765
[25] Flandin L, Verdier M, Boutherin B, Brechet Y and Cavaillé J-Y 1999 *J. Polym. Sci.* B **37** 805
[26] Cheng X, Sastry A M and Layton B E 2001 *ASME J. Eng. Mater. Technol.* **123** 12
[27] Faessel M, Delisée C, Bos F and Castéra P 2005 *Compos. Sci. Technol.* **65** 1931
[28] Broadbent S and Hammersley J 1957 *Proc. Camb. Phil. Soc.* **53** 629
[29] Kirkpatrick S 1973 *Rev. Mod. Phys.* **45** 574
[30] Balberg I, Anderson C, Alexander S and Wagner N 1984 *Phys. Rev.* B **30** 3933
[31] Berhan L and Sastry A 2007 *Phys. Rev.* E **75** 041120
[32] Berhan L and Sastry A 2007 *Phys. Rev.* E **75** 041121
[33] Nielsen L 1974 *Indust. Eng. Chem. Fundam.* **13** 17
[34] Agari Y, Ueda A and Nagai S 1993 *J. Appl. Polym. Sci.* **49** 1625
[35] Weber M and Kamal M 1997 *Polym. Compos.* **18** 711
[36] Vassal J-P, Orgéas L, Favier D, Auriault J-L and Le Corre S 2008 *Phys. Rev.* E **77** 011302
[37] Vassal J-P, Orgéas L, Favier D, Auriault J-L and Le Corre S 2008 *Phys. Rev.* E **77** 011303
[38] Bensoussan A, Lions J-L and Papanicolaou G 1978 *Asymptotic Analysis for Periodic Structures* (Amsterdam: North-Holland)
[39] Sanchez-Palencia E 1980 *Non-Homogeneous Media and Vibration Theory (Lecture Notes in Physics)* (Berlin: Springer)
[40] Auriault J-L 1991 *Int. J. Eng. Sci.* **29** 785
[41] Comsol *Multiphysics Modeling* www.comsol.fr/
[42] Le Corre S, Dumont P, Orgéas L and Favier D 2005 *J. Rheol.* **49** 1029
[43] Berhan L and Sastry A 2003 *J. Compos. Mater.* **37** 715
[44] Advani S G and Tucker C L 1987 *J. Rheol.* **3** 751
[45] Le Corre S, Caillerie D, Orgéas L and Favier D 2004 *J. Mech. Phys. Solids* **52** 395
[46] Nan C 1993 *Prog. Mater. Sci.* **37** 111
[47] Yagushi Y, Hojo H, Lee D G and Kim E G 1995 *Int. Polym. Process.* **3** 262
[48] Vincent M, Giroud T, Clarke A and Eberhardt C 2005 *Polymer* **46** 6719
[49] Dumont P, Vassal J-P, Orgéas L, Michaud V, Favier D and Månson J-E 2007 *Rheol. Acta* **46** 639
[50] Le T, Dumont P, Orgéas L, Favier D, Salvo L and Boller E 2008 *Compos. Part* A **39** 91
[51] Doi M and Edwards S F 1978 *J. Chem. Soc. Faraday Trans.* II **74** 560
[52] Ranganathan S and Advani S G 1991 *J. Rheol.* **35** 1499
[53] Toll S 1993 *J. Rheol.* **37** 123